Characterization and Analysis of Early Enzymes for Petrobactin Biosynthesis in *Bacillus anthracis*†

Brian F. Pfleger,‡ Jung Yeop Lee,‡ Ravindranadh V. Somu,§ Courtney C. Aldrich,§ Philip C. Hanna,|| and David H. Sherman*,‡,||

Life Sciences Institute and Departments of Medicinal Chemistry and Chemistry, University of Michigan, Ann Arbor, Michigan 48109, Center for Drug Design, Academic Health Center, University of Minnesota, Minneapolis, Minnesota 55455, and Department of Microbiology and Immunology, University of Michigan Medical School, Ann Arbor, Michigan 48109

Received November 20, 2006; Revised Manuscript Received January 3, 2007

ABSTRACT: Recently, iron acquisition and, more specifically, enzymes involved in siderophore biosynthesis have become attractive targets for discovery of new antibiotics. Accordingly, targeted inhibition of the biosynthesis of petrobactin, a virulence-associated siderophore encoded by the *asb* locus in *Bacillus anthracis*, may hold promise as a potential therapy against anthrax. This study describes the biochemical characterization of AsbC, the first reported 3,4-dihydroxybenzoic acid-AMP ligase, and a key component in the biosynthesis of DHB-spermidine (DHB-SP), the first isolable intermediate in petrobactin biosynthesis. AsbC catalyzes adenylation to the corresponding AMP ester of the unusual precursor 3,4-dihydroxybenzoate, in addition to benzoate substrates bearing hydrogen bond-donating substituents at the para and meta positions on the phenyl ring. In a second reaction, AsbC catalyzes transfer of the activated starter unit to AsbD, an aryl carrier protein similar to acyl and peptidyl carrier proteins that function in fatty acid, polyketide, and nonribosomal peptide biosynthesis. A third protein, AsbE, is shown to be responsible for condensation of 3,4-dihydroxybenzoyl-AsbD with spermidine, providing the DHB-spermidine arms that are linked to citrate for assembly of petrobactin. On the basis of the selective substrate profile of AsbC, a nonhydrolyzable analogue of 3,4-DHB-AMP was synthesized and shown to effectively inhibit AsbC function in vitro.

Of the known bioterror agents, *Bacillus anthracis* is widely accepted as one of the most serious threats. The resilience of the *B. anthracis* spore, the efficiency with which it infects as an aerosol, and the potential for causing lethal infections make it a formidable weapon (*1*). Apart from a mild flu-like malaise during the early stages of infection, often the first overt sign of the disease can be death. Efficacy of antibiotic therapy depends on early recognition of exposure and a prolonged (≥6 weeks) course of drugs to ensure total clearance of endospores that are unaffected by antibiotics while dormant (*2*). Vaccination offers more hope for prevention of anthrax, yet current vaccines are considered suboptimal (*3*). In addition, there are genuine concerns over the potential for deliberate development of drug resistant Select Agents for use in acts of bioterrorism. This is particularly relevant for anthrax in that resistance to most, or even all, of the antibiotic classes currently used to treat *B. anthracis* infections might theoretically be obtained without any requirement for either advanced scientific knowledge or modern molecular technologies. Furthermore, potential exists for design and generation of modified strains of *B. anthracis* that would be resistant to the current toxoid-based vaccine. Accordingly, there is a clear need for both a vaccine that affords better protection and new antibiotics that are more efficient at blocking early stages of *B. anthracis* pathogenesis.

Sufficient iron availability is a critical factor in bacterial pathogenesis as nearly all bacteria require this essential nutrient (*4*−*7*). Although iron is present in abundance, it is unavailable due to its presence as insoluble iron oxyhydroxide polymers under aerobic conditions at biological pH. Ferric iron (Fe^{3+}) solubility under these conditions is 10^{-17} M, whereas cytoplasmic iron concentrations are approximately 10^{-7} M in metabolically active microbes (*8*). The difference in concentration illustrates that uptake by diffusion is not an effective mechanism for these bacteria. To combat this challenge, many microorganisms express high-affinity iron transport systems. In general, these systems are made up of several components, including siderophores, outer membrane receptor proteins, periplasmic binding proteins, ATP dependent ABC-type transporters, and the TonB−ExbB−ExbD protein complex, each vital to the success of the transport system (*4*, *7*, *9*−*12*). Siderophores, low-molecular mass compounds (600−1500 Da) that chelate ferric iron with an extremely high affinity ($K_f \sim 10^{22}-10^{50}$) (*7*), play a central role by being secreted into the environment to scavenge free iron prior to active re-uptake where it is released.

† This work was supported by a development grant from the Great Lakes Regional Center of Excellence (GLRCE) for Bio-defense and Emerging Infectious Diseases Research (U54AI57153) and the J. G. Searle Professorship (to D.H.S.). B.F.P. is the recipient of a GLRCE postdoctoral training fellowship.

* To whom correspondence should be addressed: Life Sciences Institute, University of Michigan, 210 Washtenaw Ave., Ann Arbor, MI 48109-2216. Telephone: (734) 615-9907. E-mail: davidhs@umich.edu.

‡ University of Michigan.

§ University of Minnesota.

|| University of Michigan Medical School.

10.1021/bi6023995 CCC: $37.00
Published on Web 03/09/2007

Scheme 1: Biosynthesis of Petrobactin[a]

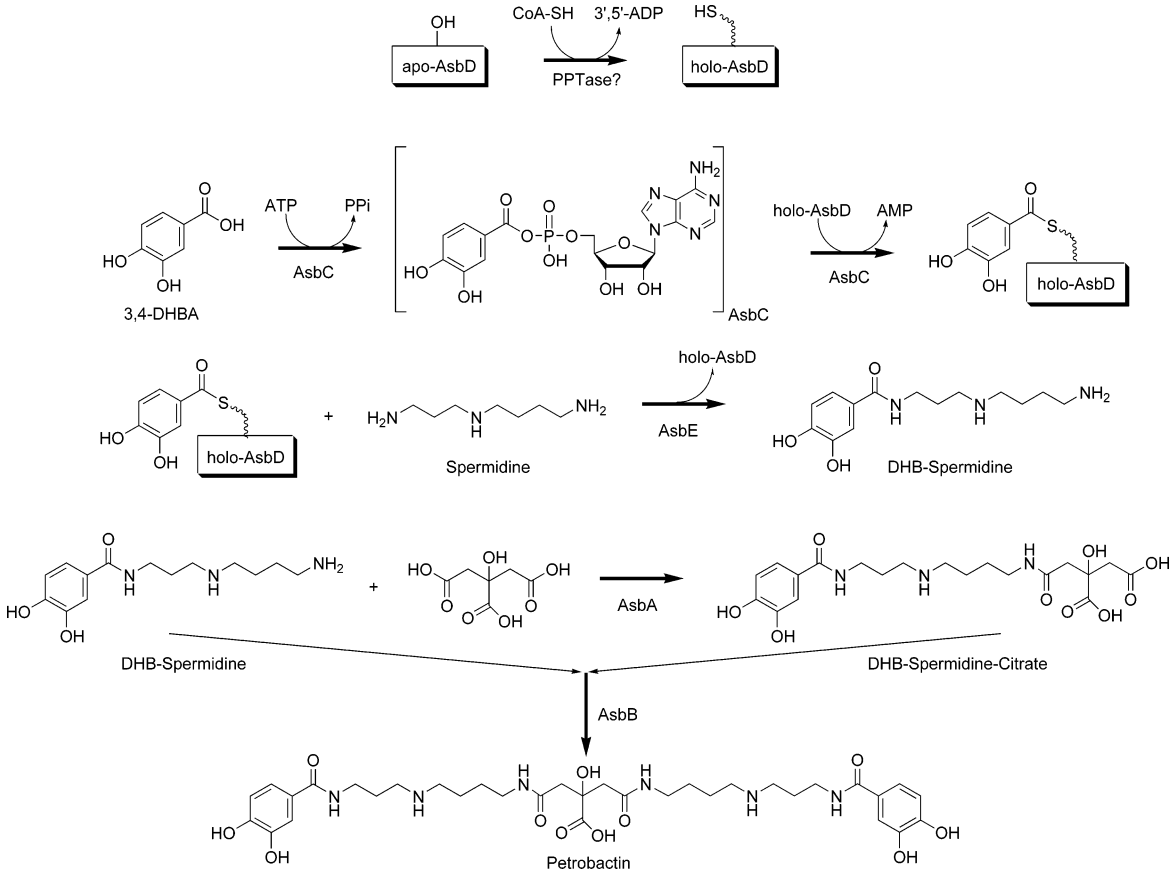

[a] 3,4-Dihydroxybenzoic acid (3,4-DHBA) is adenylated by AsbC (top left) prior to transfer to the terminal thiol of a phosphopantetheine group attached to S40 in AsbD. Phosphopantetheinylation (top center) is performed by an unidentified enzyme using coenzyme A as the source of phosphopantetheine. DHB-loaded AsbD is condensed with spermidine by AsbE to form DHB-SP. Two molecules of DHB-SP are condensed with citrate in consecutive reactions catalyzed by AsbA and AsbB, respectively (bottom), to form petrobactin.

B. anthracis produces two siderophores, petrobactin and bacillibactin, under iron-deficient conditions (*13*). The synthesis of these siderophores is associated with the expression of two gene clusters. One cluster (*bac*) has high similarity to and synteny with the *dhb* operon (*14*) in *Bacillus subtilis* that is responsible for producing a catechol-containing siderophore, bacillibactin (*15*, *16*). The second locus (*asb*) is responsible for the production of petrobactin, another catechol-based molecule whose structure is identical to a siderophore originally identified in *Marinobacter aquaeolei* (*17*−*19*). Cendrowski et al. (*13*) demonstrated that only the *asb* locus is required for growth in iron-depleted media and for virulence in a mouse model. The latter observation makes the *asb* locus a potential target of inhibitors designed to impair the growth of *B. anthracis*. This strategy has recently been supported by the discovery that petrobactin is not bound by siderocalin, an innate immune protein that binds bacillibactin as part of an antibacterial iron depletion defense (*20*). Furthermore, petrobactin has been identified as a member of a family of nonribosomal peptide synthetase (NRPS)[1] independent siderophores (*21*). Many of the members of this family have been identified from pathogenic bacteria, including virulent *Escherichia coli* (aerobactin), *Bordetella pertussis* (alcaligin), *Vibrio parahaemolyticus* (vibrioferrin), and *Staphylococcus aureus* (staphylobactin). Biochemical studies of petrobactin biosynthesis may reveal novel antimicrobial targets that are capable of effectively inhibiting siderophore synthesis from this broader group of pathogens.

In recent work, we proposed a biosynthetic pathway for petrobactin (Scheme 1) based on isolation of intermediates that accumulated in various *asb* mutant strains (*19*). In this proposed pathway, petrobactin is synthesized by condensing two molecules of 3,4-dihydroxybenzoylspermidine (DHB-SP) with citrate. Two petrobactin biosynthetic enzymes, AsbA and AsbB, were shown to be responsible for the first and second condensations, respectively. Deletion mutants of the remaining *asb* ORFs did not accumulate the DHB-SP

[1] Abbreviations: BA, benzoic acid; 2-HBA, 2-hydroxybenzoic acid; 3-HBA, 3-hydroxybenzoic acid; 4-HBA, 4-hydroxybenzoic acid; 2-CBA, 2-chlorobenzoic acid; 3-CBA, 3-chlorobenzoic acid; 4-CBA, 4-chlorobenzoic acid; 2-ABA, 2-aminobenzoic acid; 3-ABA, 3-aminobenzoic acid; 4-ABA, 4-aminobenzoic acid; 2,3-DHBA, 2,3-dihydroxybenzoic acid; 2,4-DHBA, 2,4-dihydroxybenzoic acid; 2,5-DHBA, 2,5-dihydroxybenzoic acid; 2,6-DHBA, 2,6-dihydroxybenzoic acid; 3,4-DHBA, 3,4-dihydroxybenzoic acid; 3,5-DHBA, 3,5-dihydroxybenzoic acid; 3,4-DCBA, 3,4-dichlorobenzoic acid; 3,4-DMBA, 3,4-dimethylbenzoic acid; 3C-4HBA, 3-chloro-4-hydroxybenzoic acid; 4F-3HBA, 4-fluoro-3-hydroxybenzoic acid; 3A-5HBA, 3-amino-5-hydroxybenzoic acid; DHB-AMP, 3,4-dihydroxybenzoyl-AMP or {[(2*R*,3*S*,4*R*,5*R*)-5-(6-amino-9*H*-purin-9-yl)-3,4-dihydroxytetrahydrofuran-2-yl]methylphosphoric} 3,4-dihydroxybenzoic anhydride; DHB-SP, 3,4-dihydroxybenzoylspermidine or *N*-[3-(4-aminobutylamino)propyl]-3,4-dihydroxybenzamide; NRPS, nonribosomal peptide synthetase; PPTase, phosphopantetheinyl transferase; ACP, acyl carrier protein; MESG, 2-amino-6-mercapto-7-methylpurine ribonucleoside; PNPase, purine nucleoside phosphorylase; SIM, select ion monitoring; ORF, open reading frame; arCP, aryl carrier protein; LC−MS, liquid chromatography−mass spectrometry.

intermediate observed in the Δ*asbA* and Δ*asbB* mutant strains, suggesting the products of these genes are involved in synthesizing DHB-SP. This initial study motivated our current efforts to determine the specific biochemical role for each enzyme, as well as to seek first-generation inhibitors to disrupt their function.

In the work described in this paper, *B. anthracis asb* genes were cloned into *E. coli* and recombinant Asb proteins were purified and assayed in vitro. We report the biochemical characterization and identification of a small molecule inhibitor of AsbC, the first reported 3,4-dihydroxybenzoic acid-AMP ligase, and a key component in the biosynthesis of the virulence-associated siderophore, petrobactin. AsbC is responsible for the activation of 3,4-dihydroxybenzoic acid (3,4-DHBA) prior to its condensation with spermidine. This condensation, which also requires AsbD and AsbE, generates DHB-SP, the first diffusible intermediate in the biosynthesis of petrobactin. The combined action of AsbCDE is similar to nonribosomal peptide synthesis where a carboxylic acid moiety is activated via adenylation, transferred to a carrier protein, and condensed with an amino group (*22*). Mass spectrometry analysis revealed that AsbD is an aryl carrier protein activated by phosphopantetheinylation of serine 40 of the consensus DSV motif. AsbC was shown to support ATP−[^{32}P]pyrophosphate exchange with its native substrate, 3,4-DHBA, in addition to a series of aryl analogues containing hydrogen bond donors at the 3- and/or 4-positions of the benzoyl ring. These substrates were transferred to holo-AsbD in a second reaction catalyzed by AsbC. AsbC was unable to support pyrophosphate exchange or significant transfer to AsbD utilizing 2,3-dihydroxybenzoic acid (2,3-DHBA) or 2-hydroxybenzoic acid (2-HBA), the two aryl acids found more commonly in siderophores from bacterial pathogens (*23*). Moreover, AsbE was shown to condense AsbD-linked 3,4-DHBA with spermidine to generate DHB-SP, thereby confirming the proposed biosynthetic scheme for petrobactin. A small molecule inhibitor, designed to mimic the AsbC-bound intermediate 3,4-dihydroxybenzoyl-AMP, was synthesized and shown to inhibit ATP−[^{32}P]-pyrophosphate exchange catalyzed by AsbC. Inhibitors without hydroxyl groups at the 3- and 4-positions of the benzoyl ring (benzoyl and 2-hydroxybenzoyl) failed to inhibit the AsbC-catalyzed reaction, in agreement with the substrate specificity studies. The data presented here mark the first steps toward validating petrobactin biosynthesis as a target for new small molecule therapeutics against *B. anthracis*.

METHODS

Cloning, Mutagenesis, Expression, and Protein Purification. Each *asb* ORF (Figure 1a) was amplified by high-fidelity PCR using Phusion DNA polymerase (New England Biolabs) and oligonucleotide primers (Integrated DNA Technologies) containing restriction sites outside of the start and stop codons of each gene (Table 1). PCR products were purified, digested with XhoI and NheI (New England Biolabs), and cloned into pET28b (Novagen). The *asbD*(S40A) gene was constructed by site-directed mutagenesis using a megaprimer approach (*24*). A reverse primer containing the desired change, "TCA" → "GCA", was used to generate a megaprimer consisting of the 5′-end of the gene including the desired mutation. The megaprimer was purified and used to amplify the remaining portion of *asbD*. The final PCR

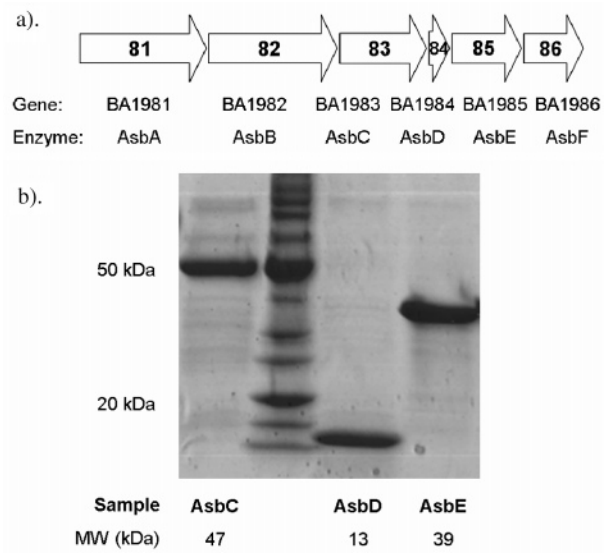

FIGURE 1: Overexpression of AsbC, AsbD, and AsbE. (a) *asb* locus showing *B. anthracis* Sterne ORFs BA1981−BA1986 encoding AsbABCDEF. (b) SDS−PAGE analysis of purified AsbC, AsbD, and AsbE. MM = Benchmark Protein Ladder (Invitrogen).

product was then cloned into pET28b as described above. Each plasmid was sequenced, and all genes contained the expected sequences except AsbC, which contained one silent mutation (^{127}GCT to ^{127}GCC, encoding A20 of AsbC).

Each construct was transformed into *E. coli* BLR(DE3) (Novagen) for protein expression. Overnight cultures were back diluted to an OD_{600} of 0.05 in LB medium containing 50 ng/mL kanamycin and grown to an OD_{600} of 0.6 at 37 °C. Cultures were then induced with 1 mM IPTG and incubated overnight at 15−18 °C. Cells concentrated by centrifugation were washed with lysis buffer [50 mM HEPES, 500 mM NaCl, and 20 mM imidazole (pH 8.0)] and disrupted by sonication. The soluble protein fraction was isolated from cellular debris following centrifugation. Ni-NTA resin (Qiagen) was incubated with the soluble fraction at 4 °C for 1 h. The resin was washed with lysis buffer and wash buffer (lysis buffer with 30 mM imidazole). Proteins were eluted with buffer containing 250 mM imidazole and 20% glycerol. Proteins were desalted into storage buffer [50 mM HEPES, 50 mM NaCl, and 20% glycerol (pH 8.0)] using gel-filtration chromatography (PD10 column, GE Healthcare) and concentrated using microconcentrators (Microcon).

In Vitro Phosphopantetheinylation of Aryl Carrier Proteins. Purified AsbD was activated in vitro using purified SVP, a promiscuous phosphopantetheinyl transferase from *Streptomyces verticillus* ATCC15003 (*25*). Activation reactions were carried out in 1 mL aliquots containing 75 mM Tris (pH 7.5), 10 mM $MgCl_2$, 2 μM SVP, 3 mM coenzyme A, and 300 μM arCP. Activated arCPs were purified into storage buffer by gel-filtration chromatography (HiPrep 26/10 desalting column, GE Healthcare) using an AKTA FPLC system (GE Healthcare). The degree of AsbD post-translational modification was examined by LC−MS. Each protein sample was buffer-exchanged into 50 mM ammonium acetate (Zeba Desalt Spin Columns, Pierce). Buffer-exchanged proteins were acidified (0.1% formic acid) prior to LC−MS analysis. Samples were separated on a Thermo-Electron Surveyor HPLC system using a Symmetry300 3.5 μm C4 column (Waters). Inline mass spectral data were

Table 1: Strains, Plasmids, and Oligonucleotides

name	sequence, genotype, or description	ref or source
E. coli BLR(DE3)	F^- *ompT hsdS*$_B$(r_B^- m_B^-) *gal dcm* (DE3) Δ(*srl-recA*)*306*::Tn*10* (Tet^R)	Novagen
pET28b	5368 bp, pBR322 origin, Kan^R, T7 promoter, His·tag (thrombin) T7·Tag MCS His·Tag	Novagen
pET28b-AsbC	pET28b with AsbC inserted in MCS with XhoI and NheI	this work
pET28b-AsbD	pET28b with AsbD inserted in MCS with XhoI and NheI	this work
pET28b-AsbD(S40A)	pET28b with AsbD(S40A) inserted in MCS with XhoI and NheI	this work
pET28b-AsbE	pET28b with AsbE inserted in MCS with XhoI and NheI	this work
pBS18	4153 bp, ColE1, ampR, T5 promoter, SVP-His·Tag	*22*
AsbC-Fwd	5′-CCCGCTAGCATGCTAATTGTTAATAGAGAAGAGTATAGC-3′	this work
AsbC-Rev	5′-CCCCTCGAGTCATGTTGTAACCTCTCCCATCTCTAG-3′	this work
AsbD-Fwd	5′-CCCGCTAGCATGAGACGGGAAGCGTTAAAGAATG-3′	this work
AsbD-Rev	5′-CCCCTCGAGTTAGTTATTCACATTTACGTCCTGTAACGG-3′	this work
AsbE-Fwd	5′-CCCGCTAGCATGACTTCAATTAAAGTGCACTGTTTAGTG-3′	this work
AsbE-Rev	5′-CCCCTCGAGTTAAAATACTAAGACAGACTCATTTGATTTCATTTC-3′	this work
AsbD-S40A-Rev	5′-TGCATCAATATATAAATCTTGATTTAAACGC-3′	this work

collected on a ThermoElectron Finnigan LTQ linear ion trap. Samples were separated using a gradient of water (0.05% trifluoroacetic acid and 0.05% formic acid) and acetonitrile (0.05% trifluoroacetic acid and 0.05% formic acid) changing from 80% water to 98% acetonitrile over 20 min. Data for ions between *m*/*z* 650 and 1800 were collected continuously.

ATP−[^{32}P]Pyrophosphate Exchange Assay. To examine the reversible activation of 3,4-DHBA and its analogues by AsbC, an ATP−[^{32}P]pyrophosphate exchange assay was performed (*26*). Reaction mixtures contained 75 mM Tris-HCl (pH 7.5), 10 mM $MgCl_2$, 5 mM DTE, 5 mM ATP, 1 mM cold $Na_4P_2O_7$, and 1 μM AsbC. Substrates were added to the mix described above in a total volume of 90 μL and incubated for 20 min at room temperature prior to the addition of 0.28 μCi of ^{32}P-labeled $Na_4P_2O_7$ in 10 μL. Reaction mixtures were incubated for 60 min before reactions were quenched with 200 μL of a solution containing 350 mM perchloric acid, 100 mM cold $Na_4P_2O_7$, and 1.7% (w/v) activated charcoal. The charcoal was pelleted by centrifugation, and the supernatant was removed prior to washing with quenching solution without charcoal. The pellet was washed twice before 500 μL of water was added to transfer the charcoal to a scintillation vial for counting. The substrate specificity of AsbC was probed in a similar manner by incubating substrates (10 μM) with the mixtures described above. Inhibition studies were also performed with ATP−$^{32}PP_i$ exchange. A dilution series (10 μL) of inhibitor in DMSO was added to the remaining reaction components described above in a total volume of 80 μL. The assay was performed as described above with 200 nM AsbC. The data acquired for compound **1** were fit to the Hill equation (*27*) $v_i/v_o = 1/[1 + ([I]/IC_{50})^h]$, where v_i is the rate of ATP−$^{32}PP_i$ exchange and v_o is the rate in the absence of inhibitor.

Continuous Spectroscopic Measurement of AsbC ATPase Activity. The noncatalytic release of phosphate by AsbC-catalyzed cleavage of ATP was monitored with a continuous spectroscopic assay. This assay (*28*) measures the spectroscopic shift corresponding to the purine nucleoside phosphorylase (PNP)-catalyzed cleavage of MESG by phosphate. Reaction mixtures (80 μL) were comprised of 75 mM Tris-HCl (pH 7.5), 10 mM $MgCl_2$, 5 mM DTE, 1 unit/mL PNP, 200 μM MESG, and 0.5 μM AsbC. The reaction was started with 8 μL of a dilution series of ATP. The absorbance at 360 nm was monitored for 30 min in a Molecular Devices Spectramax M5 device.

LC−MS Analysis of AsbD Loading. The loading of holo-AsbD by AsbC with alternative substrates was assayed by LC−MS. Reaction mixtures (100 μL) containing 75 mM Tris-HCl (pH 7.5), 10 mM $MgCl_2$, 5 mM DTE, 5 mM ATP, 50 μM holo-AsbD, 1.0 μM AsbC, and 500 μM substrate were incubated overnight at room temperature. Prior to LC−MS analysis, each sample was buffer-exchanged into 50 mM ammonium acetate (Zeba Desalt Spin Column, Pierce). LC−MS analysis was performed as described above.

LC−MS Analysis of the AsbE Condensation Reaction. In vitro production of DHB-SP was performed at room temperature for 3 h in mixtures containing 75 mM Tris-HCl (pH 7.5), 10 mM $MgCl_2$, 5 mM DTE, 5 mM ATP, 500 μM 3,4-DHBA, 500 μM spermidine, 50 μM holo-AsbD, 1.0 μM AsbC, and 5.0 μM AsbE. Reactions were terminated with the addition of 9 reaction volumes of ice-cold methanol. Proteins were separated by centrifugation, and the supernatant was transferred to a fresh tube. After the methanol extracts evaporated to dryness, the products were resuspended in 100 μL of a 50% MeOH/water mixture and acidified with 0.1% formic acid. The products of reaction mixtures containing subsets of AsbCDE were separated isocratically by liquid chromatography in 95% water (with 0.1% formic acid) and 5% methanol (with 0.1% formic acid) on an analytical reverse phase column (Xbridge C18, 3.5 μm, 2.1 mm × 150 mm, Waters). Mass spectral data were collected on a Shimadzu LCMS-2010A instrument in SIM mode monitoring *m*/*z* 282.2 ± 1.

Chemistry General Procedures. All commercial reagents (Sigma-Aldrich, Acros) were used as provided unless otherwise indicated. An anhydrous solvent dispensing system (J. C. Meyer) using two packed columns of neutral alumina was employed for drying THF and two packed columns of 4 Å MS for drying DMF, and the solvents were dispensed under argon. Anhydrous DME was purchased from Aldrich and used as provided. Flash chromatography was performed with Silica P grade silica gel 60 (Silicycle) with the indicated solvent system. All reactions were performed under an inert atmosphere of dry argon or nitrogen gas in oven-dried (150 °C) glassware. ^{1}H and ^{13}C NMR spectra were recorded on a Varian 600 MHz spectrometer. Proton chemical shifts are reported in parts per million from an internal standard of residual chloroform (7.26 ppm) or methanol (3.31 ppm), and carbon chemical shifts are reported using an internal standard of residual chloroform (77.0 ppm) or methanol (49.1 ppm). Proton chemical data are reported as follows: chemical shift, multiplicity (s, singlet; d, doublet; t, triplet; q, quartet; p, pentet; m, multiplet; and br, broad), coupling constant, integration. High-resolution mass spectra were obtained on

an Agilent TOF II TOF/MS instrument equipped with either an ESI or APCI interface. Optical rotations were measured on a Rudolph Autopol III polarimeter. Melting points were measured on electrothermal Mel-Temp manual melting point apparatus and are uncorrected.

*N-Hydroxysuccinimidyl 3,4-Dibenzyloxybenzoate (**4**).* To a solution of 3,4-dibenzyloxybenzoic acid (*29*) (1.0 g, 3.0 mmol, 1.0 equiv) in THF (30 mL) at 0 °C were added *N*-hydroxysuccinimide (0.34 g, 3.0 mmol, 1.0 equiv) and DCC (0.62 g, 3.0 mmol, 1.0 equiv). The resulting mixture was stirred for 30 min at 0 °C and then for 2 h at room temperature. The reaction mixture was filtered to remove the DCU precipitate, and the filtrate was concentrated under reduced pressure. Purification by flash chromatography (4:1 EtOAc/hexane) afforded the title compound (1.19 g, 92%) as a white solid: mp 134−136 °C; $R_f = 0.80$ (3:7 EtOAc/hexanes); ^{1}H NMR (600 MHz, $CDCl_3$) δ 2.86 (br s, 4H), 5.17 (s, 2H), 5.24 (s, 2H), 7.96 (d, $J = 9.0$ Hz, 1H), 7.28−7.34 (m, 2H), 7.34−7.40 (m, 4H), 7.40−7.48 (m, 4H), 7.67 (br s, 1H), 7.75 (dd, $J = 8.4$, 1.8 Hz, 1H); ^{13}C NMR ($CDCl_3$, 75 MHz) δ 25.9, 71.1, 71.6, 113.5, 116.1, 117.6, 125.9, 127.4, 129.7, 128.3, 128.4, 128.8, 128.9, 136.3, 136.7, 148.9, 154.8, 161.7, 169.7.

*5′-O-[N-(3,4-Dibenzyloxybenzoyl)sulfamoyl]-2′,3′-O-isopropylideneadenosine (**5**).* To a solution of **3** (*30*) (0.3 g, 0.77 mmol, 1.0 equiv) in DMF (15 mL) at 0 °C was added NHS ester **4** (1.0 g, 2.33 mmol, 3.0 equiv) followed by Cs_2CO_3 (0.76 g, 2.33, 3.0 equiv), and the reaction mixture was stirred 16 h at room temperature. The reaction mixture was filtered to remove solids and washed with a small quantity of DMF. Concentration under reduced pressure and purification by flash chromatography (80:20:1 EtOAc/MeOH/Et_3N) afforded the title compounds as a thick oil (0.45 g, 92%): $R_f = 0.2$ (9:1 MeOH/EtOAc); $[\alpha]^{20}_D$ −66 (*c* 0.65, MeOH); ^{1}H NMR (600 MHz, $CDCl_3$) δ 1.31 (s, 3H), 1.56 (s, 3H), 4.26−4.36 (m, 2H), 4.52−4.58 (m, 1H), 5.07 (s, 2H), 5.10−5.16 (m, 3H), 5.32 (dd, $J = 6.0$, 3.6 Hz, 1H), 6.20 (d, $J = 3.0$ Hz, 1H), 6.94 (d, $J = 8.4$ Hz, 1H), 7.20−7.36 (m, 6H), 7.38−7.44 (m, 4H), 7.63 (d, $J = 8.4$ Hz, 1H), 7.76 (s, 1H), 8.13 (s, 1H), 8.45 (s, 1H); ^{13}C NMR (150 MHz, $CDCl_3$) δ 25.6, 27.6, 69.9, 72.1, 72.4, 83.4, 85.8, 85.9, 92.1, 114.5, 115.4, 116.7, 116.8, 120.3, 124.5, 128.7, 128.8, 128.9, 129.0, 129.5, 129.6, 138.6, 138.8, 141.6, 149.9, 150.7, 153.2, 154.1, 157.4, 174.9; HRMS (ESI-) calcd for $C_{34}H_{33}N_6O_9S$ [M − H]$^-$ 701.2035, found 701.2027 (error, 1.1 ppm).

*5′-O-[N-(3,4-Dihydroxybenzoyl)sulfamoyl]-2′,3′-O-isopropylideneadenosine (**6**).* To a solution of **5** (0.41 g, 0.58 mmol) in MeOH (20 mL) was added 10% Pd/C (80 mg, 20% by wt), and the mixture was stirred for 12 h, under H_2 (1 atm). The reaction mixture was filtered through a plug of Celite and washed with MeOH (3 × 20 mL). The filtrate was concentrated, and purification by flash chromatography (25:75:1 MeOH/EtOAc/Et_3N) provided the product (0.23 g, 76%) as a white solid: mp >185 °C dec; $R_f = 0.15$ (1:4 MeOH/EtOAc); $[\alpha]^{20}_D$ −11.6 (*c* 0.35, MeOH); ^{1}H NMR (600 MHz, CD_3OD) δ 1.34 (s, 3H), 1.58 (s, 3H), 4.24−4.36 (m, 2H), 4.54 (d, $J = 1.8$ Hz, 1H), 5.14 (d, $J = 5.4$ Hz, 1H), 5.36 (dd, $J = 6.0$, 3.0 Hz, 1H), 6.21 (d, $J = 2.4$ Hz, 1H), 6.72 (d, $J = 8.4$ Hz, 1H), 7.45 (d, $J = 8.4$ Hz, 1H), 7.51 (s, 1H), 8.15 (s, 1H), 8.44 (s, 1H); ^{13}C NMR (150 MHz, CD_3OD) δ 25.5, 27.4, 69.7, 83.3, 85.7, 85.8, 91.9, 115.3, 115.4, 117.4, 120.1, 123.0, 130.1, 141.5, 145.5, 150.1, 150.4, 154.0, 157.3, 175.5; HRMS (ESI-) calcd for $C_{17}H_{17}N_6O_9S$ [M − H]$^-$ 521.1096, found 521.1102 (error, 1.1 ppm).

*5′-O-[N-(3,4-Dihydroxybenzoyl)sulfamoyl]adenosine (**1**).* Compound **6** (0.18 mg, 0.35 mmol, 1.0 equiv) was stirred in 80% aqueous TFA (2.0 mL) for 3 h and then concentrated in vacuo. Purification by flash chromatography (40:60:1 MeOH/EtOAc/Et_3N) afforded the title compound (120 mg, 72%) as white solid: mp >190 °C dec; $R_f = 0.1$ (2:3 MeOH/EtOAc); $[\alpha]^{20}_D$ −101 (*c* 0.49, MeOH); ^{1}H NMR (600 MHz, CD_3OD) δ 4.28−4.40 (m, 3H), 4.42 (t, $J = 3.6$ Hz, 1H), 4.71 (t, $J = 5.4$ Hz, 1H), 6.08 (d, $J = 6.0$ Hz, 1H), 6.71 (d, $J = 7.8$ Hz, 1H), 7.44 (d, $J = 7.8$ Hz, 1H), 7.50 (s, 1H), 8.15 (s, 1H), 8.51 (s, 1H); ^{13}C NMR (150 MHz, $CDCl_3$) δ 10.3, 47.5, 69.3, 72.5, 76.3, 84.8, 89.4, 115.5, 117.4, 120.3, 122.9, 130.5, 141.3, 145.6, 150.3, 150.9, 153.9, 157.3, 175.7; HRMS (ESI-) calcd for $C_{17}H_{17}N_6O_9S$ [M − H]$^-$ 481.0778, found 481.0784 (error, 1.2 ppm).

RESULTS

Cloning, Expression, and Purification of AsbCDE. In a recent analysis (*19*), we demonstrated that petrobactin is derived from a DHB-SP intermediate that accumulated in supernatants of Δ*asbA* and Δ*asbB* mutant strains of *B. anthracis* but was absent from other single-gene disruption strains (Δ*asbC*, *-D*, *-E*, and *-F*). These data suggested that the AsbCDEF enzymes (or a subset of this group) were responsible for assembly of DHB-spermidine. BLAST homology searches of AsbCDEF identified highly similar sequences relating to nonribosomal peptide synthetase catalytic domains, suggesting a thiotemplate mechanism for DHB-SP synthesis. Therefore, in vitro studies were employed to confirm the proposed role of the "early" biosynthetic enzymes in the petrobactin biosynthetic pathway.

The *asbC*, *asbD*, and *asbE* genes were cloned by PCR from genomic DNA isolated from *B. anthracis* Sterne into pET28b, an overexpression vector incorporating a C-terminal six-histidine tag into each protein. Cultures of *E. coli* BLR(DE3) harboring each overexpression construct were used to generate soluble protein that was purified by Ni-NTA affinity chromatography using standard binding, washing, and elution conditions in HEPES buffers. SDS−PAGE analysis of the purified Asb enzymes demonstrated bands corresponding to the expected size for each His-tagged protein: AsbC (47 kDa), AsbD (13 kDa), and AsbE (39 kDa) (Figure 1b).

Biochemical Characterization of AsbD. The results of BLAST searches queried against AsbD revealed strong homology to acyl, aryl, and peptidyl carrier proteins. This class of polypeptides (approximately 10−15 kDa) is involved in the biosynthesis of fatty acids, polyketides, nonribosomal peptides, and siderophores (*23*). To initiate the analysis of petrobactin biosynthesis and determine which subset of AsbCDEF produces DHB-SP, we first sought to confirm the function of AsbD. Carrier proteins contain a conserved serine residue (S40 in AsbD) to which a phosphopantetheine molecule is covalently attached (*23*). The terminal thiol of the phosphopantetheine moiety is the site of substrate loading. Activation of carrier proteins occurs post-translationally via addition of phosphopantetheine from coenzyme A catalyzed by phosphopantetheinyl transferases (PPTase) (*31*). While the genes encoding dedicated PPTases are

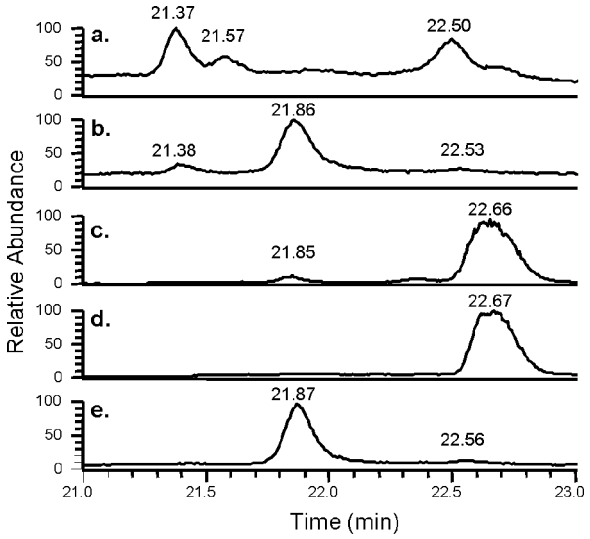

FIGURE 2: LC−MS analysis of AsbD phosphopantetheinylation. LC−MS traces of AsbD filtered for the five most abundant charge states of each protein. (a) Purified AsbD contains two peaks corresponding to its apo and holo forms; see Table 2 for deconvoluted masses. (b) AsbD incubated with SVP and coenzyme A results in nearly complete conversion to the holo form. Traces of AsbD(S40A) incubated without (c) and with (d) SVP and coenzyme A were identical, indicating S40 is the site of phosphopantetheinylation by SVP. (e) Incubation of AsbC, holo-AsbD, 3,4-DHBA, and ATP results in formation of 3,4-DHB-loaded AsbD.

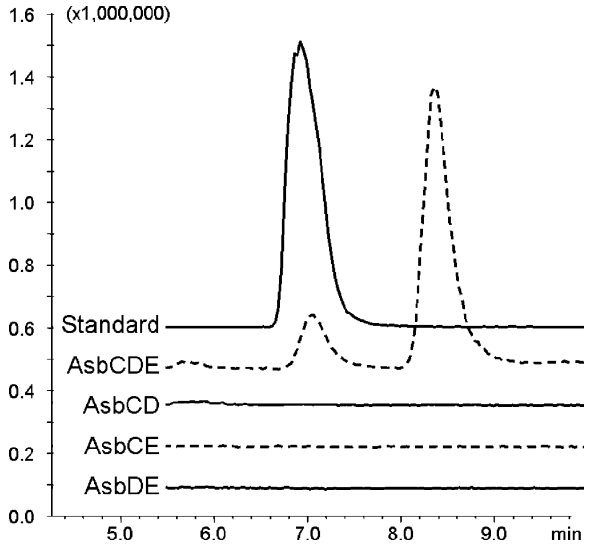

FIGURE 3: In vitro biosynthesis of DHB-SP. LC−MS traces (SIM of the ion at *m*/*z* 282.2) show the presence of DHB-SP in reaction mixtures containing the combination of all three enzymes, AsbCDE. No pairwise combination is capable of generating a peak with the correct *m*/*z* for DHB-SP. The combination of AsbCDE also generates a second species that fragments differently from the DHB-SP standard and contains daughter ions corresponding to a DHB-SP isomer (B. F. Pfleger and D. H. Sherman, unpublished results).

frequently encoded within secondary metabolite clusters (*32*, *33*), an evident homologue is not encoded within the *asb* cluster. It is likely that, in vivo, the enzyme encoded by BA2375 [a homologue of *B. subtilis* Sfp (*34*)] catalyzes the reaction. In vitro modification of carrier proteins can be performed with Sfp and other promiscuous PPTases, including SVP from *S. verticillus* ATCC15003 (*25*).

To confirm the role of AsbD as a presumed aryl carrier protein, in vitro phosphopantetheinylation reactions were performed using SVP and coenzyme A. The apo and holo forms of AsbD were separated via liquid chromatography and monitored with an ion trap mass spectrometer. A peak corresponding to an envelope of charge states from apo AsbD was detected at 22.5 min. Both the holo and 3,4-DHBA-loaded forms of AsbD eluted earlier in two peaks with retention times of 21.4 and 21.9 min. Each of these peaks contained the same series of ions; only their relative intensities were different (data not shown). Purified AsbD from recombinant *E. coli* resulted in a mixed population of apo and holo forms at a ratio of approximately 3:1 (Figure 2 and Table 2), suggesting that native *E. coli* PPtases can utilize AsbD as a substrate. After incubation with coenzyme A and purified SVP, this ratio changed to approximately 1:14 (apo:holo). The deconvoluted masses for each of these peaks corresponded to the expected masses of the apo (12 949 Da) and holo (13 289 Da) forms of AsbD (missing its N-terminal methionine).

A point mutation converting the essential serine residue to alanine (S40A) was generated to confirm the site of phosphopantetheinylation in AsbD. The purified S40A mutant protein was eluted at 22.6 min (Figure 2c,d and Table 2) with a spectrum of charge states that when deconvoluted agreed with the expected mass of AsbD(S40A) (12 935 Da). In vitro incubation with SVP and coenzyme A did not change the retention time or envelope of charge states, supporting the hypothesis that S40 is the site of phosphopantetheinylation. Together, these data confirm that AsbD is a carrier protein analogous to previously described aryl, acyl, and peptidyl carrier proteins.

Production of DHB-SP. In an effort to determine which subset of AsbCDEF produced DHB-SP, mixtures of AsbC, holo-AsbD, AsbE, 3,4-DHBA, spermidine, and ATP were incubated for 3 h. LC−MS traces of these reactions contained two peaks, at 7.0 and 8.3 min (Figure 3). These peaks contained the characteristic absorbance signature of 3,4-DHBA (data not shown). The smaller peak at 7.0 min had a retention time identical to that of a synthesized DHB-SP standard (*19*) (Figure 3). The second, larger peak at a retention time of 8.3 min has an MS/MS fragmentation pattern consistent with an isomer of DHB-SP with the DHBA group attached to the four-carbon chain terminus of spermidine (B. F. Pfleger and D. H. Sherman, unpublished results). A peak with this fragmentation pattern was also found in supernatants of Δ*asbA* and Δ*asbB* mutants (*19*). Pairwise combinations of AsbCDE (e.g., AsbCD, AsbCE,

Table 2: Mass Spectrometric Analysis of AsbD Phosphopantetheinylation

Figure 2 panel	protein	expected mass (Da)	deconvoluted mass (Da)		holo:apo ratio
a	AsbD	12 949.0	12 950.4 ± 0.7	13 288.2 ± 1.7	1:3
b	AsbD with SVP	13 289.0	12 950.4 ± 2.9	13 291.5 ± 0.7	14:1
c	AsbD(S40A)	12 935.0	12 935.5 ± 0.7		
d	AsbD(S40A) with SVP	13 274.0	12 935.4 ± 0.7		
e	loaded AsbD	13 426.3	13 424.8 ± 0.5		

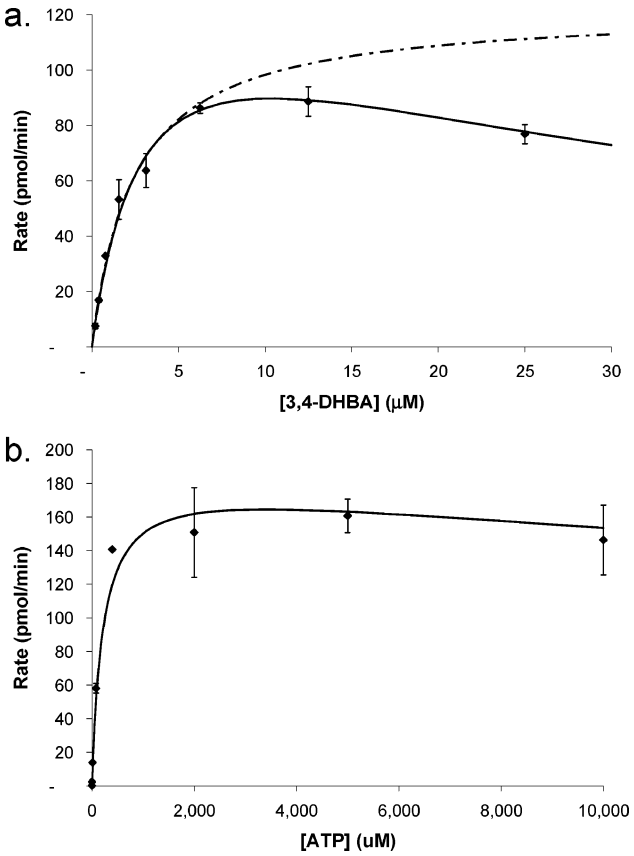

FIGURE 4: ATP−$^{32}PP_i$ exchange kinetics of AsbC. (a) Dependence of ATP−$^{32}PP_i$ exchange on 3,4-DHBA fit to a substrate-inhibited model (—) and Michaelis−Menten model (-•-). (b) Dependence on ATP fit with a substrate-inhibited model.

and AsbDE) with 3,4-DHBA, spermidine, and ATP failed to generate either product (Figure 3), confirming the involvement of each enzyme in DHB-SP biosynthesis.

Adenylation of 3,4-DHBA by AsbC. Although analysis of specific *asb* mutant strains provided significant insights into late stage enzymes in petrobactin assembly (*19*), some questions regarding the function of AsbC and AsbE remained. This motivated our efforts to establish which enzyme catalyzed activation of 3,4-DHBA and which one mediated condensation of the aryl AsbD with spermidine. BLAST homology searches revealed that AsbC was similar to AMP-ligases, including *E. coli*-encoded EntE (*35*) and *Vibrio cholerae*-encoded VibE (*26*), which perform similar adenylation steps in the biosynthesis of the siderophores enterobactin and vibriobactin, respectively. To confirm the functional role of AsbC, incubation of either AsbC or AsbE with holo-AsbD, 3,4-DHBA, and ATP was analyzed via LC−MS to assess AsbD loading. The AsbC reaction returned an envelope of ions that corresponded to the expected mass for DHBA-modified AsbD (13 426 Da) (Figure 2 and Table 2). The AsbE reaction under otherwise identical conditions gave a trace and charge envelope identical to those of holo-AsbD (data not shown), confirming that AsbC performs the adenylation and transfer of 3,4-DHBA to holo-AsbD.

ATP−[^{32}P]pyrophosphate exchange (*26*) was performed to estimate the rate of adenylation. Rates of [^{32}P]ATP formation were determined from end-point assays following a 60 min incubation at room temperature. Because of reduced rates observed at high substrate concentrations, the kinetic data were fit to a substrate-inhibited model (Figure 4). This fit generated a K_m of 3.1 μM for DHBA and 216 μM for ATP (Table 3), similar to those determined for EntE (2.7 μM), VibE (0.46 μM), and YbtE (4.6 μM) with their native substrates (*26*, *35*, *36*). The AsbC K_{cat} values for 3,4-DHBA and ATP were determined to be 7.1 and 9.1 min^{-1}, respectively, which are significantly slower than those of EntE (330 min^{-1}), VibE (138 min^{-1}), and YbtE (230 min^{-1}) with their native substrates (Table 3). The substrate inhibition constant, K_i, was determined to be 35 μM for DHBA and 54 mM for ATP (Table 3).

Table 3: ATP−$^{32}PP_i$ Exchange Kinetic Parameters

enzyme	K_{cat} (min^{-1})	K_m (μM)	K_I (μM)	K_{cat}/K_m (μM^{-1} min^{-1})
substrate				
AsbC (3,4-DHBA)	7.1	3.1	35	2.3
EntE (2,3-DHBA)[a]	330	2.7		122
VibE (2,3-DHBA)[a]	138	0.46		300
YbtE (2-HBA)[b]	230	4.6		50
ATP				
AsbC (3,4-DHBA)	9.1	216	54000	0.04
EntE (2,3-DHBA)[c]	350	1120		0.31
YbtE (2-HBA)[b]	270	350		0.77

[a] See ref *26*. [b] See ref *35*. [c] See ref *36*.

AsbC Substrate Specificity. In an effort to gain insight into the critical interactions responsible for ligand binding, the AsbC substrate specificity was probed using an ATP−$^{32}PP_i$ exchange assay. As expected, the native substrate (3,4-DHBA) supported the greatest rate of PP_i exchange, whereas most other benzoic acid analogues appeared to be poor substrates (Figure 5). The limited number of substrates that also generated significant [^{32}P]ATP included 4-hydroxybenzoic acid (4-HBA), 3-hydroxybenzoic acid (3-HBA), 3,5-dihydroxybenzoic acid (3,5-DHBA), 3-amino-5-hydroxybenzoic acid (3A-5HBA), 3-chloro-4-hydroxybenzoic acid (3C-4HBA), and 4-fluoro-3-hydroxybenzoic acid (4F-3HBA) (Figure 5). These substrates all contain hydrogen bond-donating groups at the 3- or 4-position of the benzoic acid moiety. Replacement of these groups with nondonating polar groups abolished activity. Interestingly, 2,3-dihydroxybenzoic acid, a component of bacillibactin in *B. anthracis*, does not support significant ATP−$^{32}PP_i$ exchange, indicating that AsbC discriminates between the two available forms of DHBA. As expected, the substrate specificity of AsbC differs from that of EntE, which utilizes 2,3-DHBA as its preferred substrate (*37*), but the decrease in rate from strongly to weakly bound substrates is similar in magnitude.

In the absence of substrate, AsbC was able to catalyze pyrophosphate exchange (Figure 5), suggestive of reversible ATPase activity. This activity was confirmed by performing a coupled spectroscopic assay to monitor phosphate release. In this experiment, phosphate released into solution is used to cleave MESG (2-amino-6-mercapto-7-methylpurine ribonucleoside) into ribose 1-phosphate and 2-amino-6-mercapto-7-methylpurine in a reaction catalyzed by purine nucleoside phosphorylase (PNPase) (*28*). This cleavage results in a shift in absorbance that can be monitored at 360 nm. Reaction mixtures containing PNPase, MESG, AsbC, and ATP resulted in a series of increasing curvilinear absorbance readings (data not shown), confirming that AsbC catalyzes release of phosphate in the absence of substrate.

Table 4: AsbC Substrate Specificities for Transfer to Holo-AsbD

substrate	abbreviation	loaded	expected mass (Da)	deconvoluted masses (Da)	
holo-AsbD			13 290.3	13 289.2 ± 1.2	
benzoic acid	BA	no	13 394.3	13 287.5 ± 0.7	
2-hydroxybenzoic acid	2-HBA	no	13 410.3	13 288.2 ± 0.5	
3-hydroxybenzoic acid	3-HBA	yes	13 410.3	13 408.9 ± 1.2	
4-hydroxybenzoic acid	4-HBA	yes	13 410.3	13 410.3 ± 0.5	
2-chlorobenzoic acid	2-CBA	no	13 428.3	13 288.3 ± 0.7	
3-chlorobenzoic acid	3-CBA	no	13 428.3	13 287.8 ± 0.9	
4-chlorobenzoic acid	4-CBA	no	13 428.3	13 288.1 ± 0.4	
2-aminobenzoic acid	2-ABA	partial	13 409.3	13 403.2 ± 1.5	13 287.8 ± 1.0
3-aminobenzoic acid	3-ABA	partial	13 409.3	13 406.0 ± 1.1	13 288.4 ± 0.7
4-aminobenzoic acid	4-ABA	partial	13 409.3	13 408.0 ± 1.1	13 288.6 ± 0.9
2,3-dihydroxybenzoic acid	2,3-DHBA	partial	13 426.3	13 427.2 ± 1.8	13 288.8 ± 1.8
2,4-dihydroxybenzoic acid	2,4-DHBA	partial	13 426.3	13 424.0 ± 1.6	13 287.0 ± 2.9
2,5-dihydroxybenzoic acid	2,5-DHBA	no	13 426.3	13 289.7 ± 0.6	
2,6-dihydroxybenzoic acid	2,6-DHBA	no	13 426.3	13 288.8 ± 1.2	
3,4-dihydroxybenzoic acid	3,4-DHBA	yes	13 426.3	13 424.8 ± 0.5	
3,5-dihydroxybenzoic acid	3,5-DHBA	yes	13 426.3	13 426.2 ± 1.7	
3,4-dichlorobenzoic acid	3,4-DCBA	no	13 462.2	13 288.3 ± 0.5	
3,4-dimethylbenzoic acid	3,4-DMBA	no	13 422.3	13 288.4 ± 0.6	
3-chloro-4-hydroxybenzoic acid	3C-4HBA	yes	13 444.3	13 444.8 ± 0.4	
4-fluoro-3-hydroxybenzoic acid	4F-3HBA	yes	13 428.3	13 427.8 ± 2.3	
3-amino-5-hydroxybenzoic acid	3A-5HBA	yes	13 425.3	13 424.4 ± 0.9	

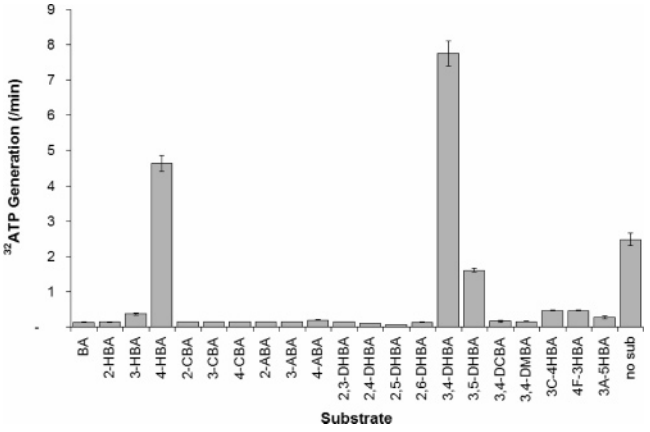

FIGURE 5: AsbC substrate specificity determined by ATP−$^{32}PP_i$ exchange. Substitutions at the meta and para positions on the phenyl ring appear to be the most important for adenylation. Substrates with hydroxyl groups at these positions supported the greatest rate of ATP−$^{32}PP_i$ exchange. Non-hydrogen bond donors at these positions did not support exchange. Substitution at the ortho position did not support ATP−$^{32}PP_i$ exchange and removed any benefit provided by additional hydroxyl groups positioned elsewhere on the ring. AsbC generated significant quantities of [^{32}P]ATP in the absence of substrate. This ATPase activity was confirmed by a coupled spectroscopic assay for phosphate release (data not shown).

AsbC is responsible for two reactions, the adenylation of a 3,4-DHBA and transfer to holo-AsbD. Any adenylated substrate that cannot be transferred would theoretically remain in the active site and function as a competitive inhibitor. Because the pyrophosphate exchange assays revealed that AsbC is capable of adenylating several substrates, we examined the ability of AsbC to transfer these alternate substrates to holo-AsbD and assess whether any would function as inhibitors. Aryl group transfer to AsbD was assessed by LC−MS analysis of overnight incubations of substrate, ATP, AsbC, and holo-AsbD. All of the substrates that supported ATP−$^{32}PP_i$ exchange were found to have an envelope of charge states that corresponded to the expected mass for loaded AsbD (Table 4), indicating that none were capable of competitively inhibiting AsbC. Interestingly, several substrates that did not support ATP−$^{32}PP_i$ exchange to a significant degree were found to partially load holo-AsbD. In these samples, the envelope of charge states contained ions representing the holo and arylated forms of the carrier protein. Among the partially loaded substrates were 2,3- and 2,4-DHBA, as well as 2-, 3-, and 4-aminobenzoic acid. Together, these data emphasize the flexibility of AsbC and the importance of utilizing hydrogen bonding donors at the 3- and 4-positions to maximize the binding affinity for potential inhibitors.

Inhibition of AsbC with Intermediate Analogues. Adenylation domains such as AsbC are known to tightly bind adenylated substrates prior to phosphopantetheine-mediated transesterification, resulting in loaded carrier protein. This tight binding provides a potentially useful mechanism-based strategy for the design of competitive inhibitors. To explore this approach, three acylsulfamate structures that mimic the DHB-AMP intermediate of AsbC were synthesized. An ATP−[^{32}P]pyrophosphate assay was then performed to test the molecule mimicking the native substrate, bearing the 3,4-dihydroxybenzoic group (**1**), against variants that bear a benzoic acid (**7**) or 2-hydroxybenzoic acid group (**8**).

Synthesis of inhibitor **1** was achieved starting from 2′,3′-*O*-isopropylidene adenosine (*2*). Sulfamoylation (*29*) of **2** provided **3**, which was coupled with **4** in the presence of Cs_2CO_3 to afford **5**. Sequential deprotection of the benzyl ethers with Pd/C and the acetonide with aqueous TFA provided the required inhibitor **1** in 46% overall yield over four steps (Scheme 2).

The rates of ATP−$^{32}PP_i$ exchange in the presence of each inhibitor are shown in Figure 6. Compound **1** was able to inhibit the reaction with an IC_{50} of ~250 nM (using a Hill coefficient of 0.68). This value is comparable to those seen in inhibitor studies of MbtA, but they are less potent than the best inhibitors reported in those studies (*30*, *38*−*40*). Not surprisingly, acylsulfamate structures **7** and **8** failed to inhibit ATP−$^{32}PP_i$ exchange in vitro, supporting the substrate specificity profile obtained for AsbC. The absence of hydrogen bond donors at the 3- and 4-positions of the benzoic acid moiety are clearly significant for binding as well as adenylation and transfer. Future structure−activity relation-

Scheme 2: Chemical Synthesis of AsbC Inhibitors

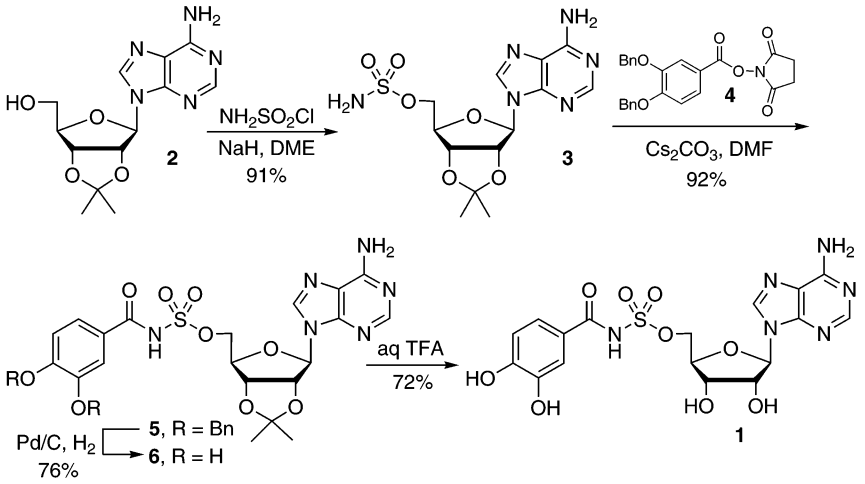

ship studies will be designed to explore other regions of inhibitor **1** while maintaining the 3,4-dihydroxy moiety to maximize binding affinity.

DISCUSSION

Petrobactin is a virulence-associated siderophore in *B. anthracis* whose biosynthetic enzymes represent potential targets for development of new anti-infective agents. The cellular assembly of petrobactin occurs in two distinct phases, each containing potential targets for inhibitor discovery. The ultimate synthesis utilizes two molecules of DHB-SP in consecutive condensations with two terminal carboxylic acids of citrate. The substrate, intermediate, and product of these condensations are diffusible compounds that have been isolated from supernatants of *B. anthracis* strains bearing the corresponding *asb* deletion mutants (*19*). Formation of the final amide bonds with a central citrate is the defining characteristic of a new NRPS independent family of siderophores (*21*). This family of enzymes is found in many bacterial genomes and may provide a target for development of therapeutics against specific microbial pathogens, including *B. anthracis*, as well as *E. coli*, *Bo. pertussis*, *V. parahaemolyticus*, and *St. aureus*. Currently, little is known about the molecular mechanism or structure of these important enzymes. Structural and mutagenesis studies of AsbA and AsbB, the NRPS independent enzymes involved in petrobactin biosynthesis, might reveal the biochemical mechanism utilized by this family and facilitate the identification of effective antibiotics.

Although petrobactin is considered a member of the NRPS independent family of siderophores (*21*), its early intermediate is synthesized by three enzymes that share a high degree of homology and mechanistic similarity to nonribosomal peptide synthetase catalytic domains. In the first stage of biosynthesis, AsbCDE generate the diffusible intermediate DHB-SP through use of a carrier protein-bound 3,4-DHBA (Scheme 1). This series of reactions is similar to those utilized in the synthesis of vibriobactin and enterobactin where aryl acids are condensed with amines norspermidine (*26*) and serine (*9*), respectively.

The sequence of AsbC bears overall similarity to those of VibE (22% identical and 38% similar) (*26*) and EntE (20% identical and 36% similar) (*35*), enzymes that catalyze adenylation of 2,3-DHBA in the biosynthesis of vibriobactin and enterobactin. Many enzymes that are homologous with these three adenylation domains cluster into three groups on the basis of their substrate specificity (Figure 1 of the Supporting Information). EntE and VibE cluster together with DhbE, an enzyme that adenylates 2,3-DHBA in bacillibacin

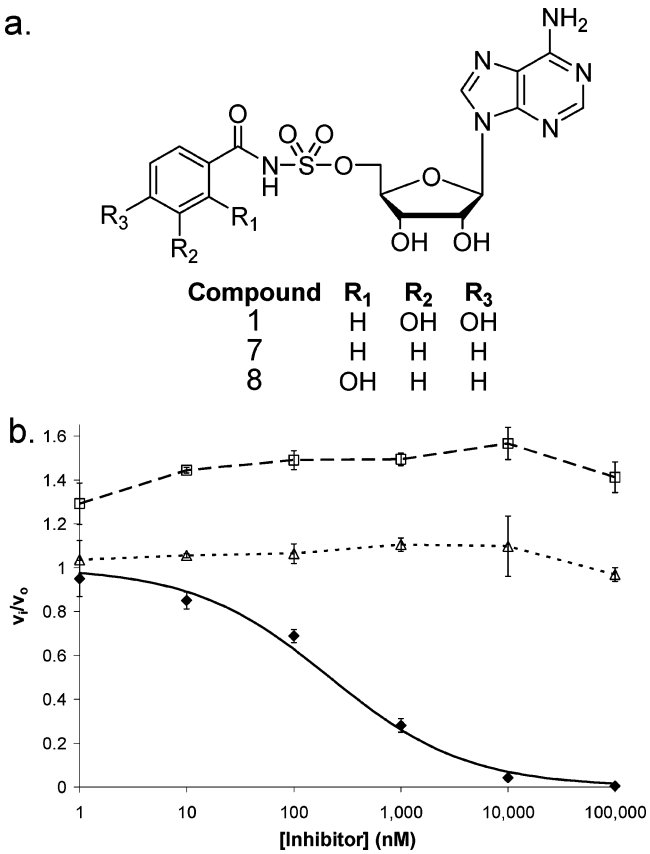

FIGURE 6: Inhibition of AsbC. (a) Structure of acylsulfamate DHB-AMP mimics. The stable acylsulfamate linkage between the aryl and nucleoside domains should prevent ATP formation and/or transfer to a phosphopantetheinyl arm. If AsbC binds one of these intermediate analogues with strong affinity, the analogues will act as a competitive inhibitor by blocking the active site. (b) ATP−$^{32}PP_i$ exchange reactions in the presence of variable concentrations of inhibitor. The presence of hydroxyl groups at the 3- and 4-positions of the benzyl portion of the inhibitor is critical for binding and inhibition: compound **1**, fit to a Hill equation with a coefficient of 0.68 (◆), compound **7** (△), and compound **8** (□).

biosynthesis in *B. subtilis* (*41*) and *B. anthracis*. The second group clusters around MbtA (*42*) and YbtE (*36*), enzymes that adenylate salicylic acid (2-HBA) in the biosynthesis of mycobactin and yersiniabactin, respectively. AsbC falls into a small third cluster with its homologue in *M. aquaeolei*, the marine bacteria from which petrobactin was first identified (*43*), and an enzyme in *Rhodopseudomonas palustris* (*44*). A crystal structure of DhbE aligned with an analogous structure of PheA, a phenylalanine adenylation domain, has been used to define the specificity residues for the cluster of 2,3-DHBA and 2-HBA adenylating enzymes (*41*). AsbC and its clustered homologues have a different set of residues in the substrate specificity defining positions. These key AsbC residues (SYCYMSY) may define the analogous interactions for 3,4-DHBA specific adenylation domains. Crystal structures of AsbC with bound ligand as well as site-directed mutagenesis will be needed to validate interactions between these residues and 3,4-DHBA and/or AMP/ATP.

Our study shows that AsbC can be inhibited by acylsulfamate analogues, based on its native intermediate, DHB-AMP. This strategy has been useful for identifying inhibitors of enzymes with similar mechanisms, including tRNA synthetases (*45*), MbtA (*30*, *38*−*40*), and YbtE (*39*). While the observed inhibition of AsbC by **1** was moderate ($IC_{50} = 250$ nM) compared to those identified against related enzymes from previous studies ($IC_{50} \sim 10$ nM) (*39*, *40*), the success of this approach warrants further structure−activity relationship analysis. From the substrate specificity and inhibition studies reported here, it is evident that the presence of hydrogen bond donors at the 3- and 4-positions of the benzoyl moiety are essential for binding, adenylation, and aryl transfer. Future studies with inhibitors related to **1** will examine the effects of alternative regions of the molecule on binding and enzyme inhibition. Crystal structures of AsbC containing either substrate or inhibitor would greatly facilitate these studies and provide additional insights into interactions between key active site amino acid residues and the 3- and 4-hydroxyl groups on the phenyl ring.

In addition to AsbC, we have identified AsbE as a potential target of small molecule inhibitors against petrobactin biosynthesis. We have shown that AsbE condenses 3,4-DHB-loaded AsbD with spermidine. AsbE has homologues in both *M. aquaeolei* (*43*) and *R. palustris* (*44*) but shows little similarity to other polypeptides in the protein databases. Biochemical and crystallographic studies of this enzyme might reveal effective strategies for inhibitor design. It is intriguing that AsbE catalyzes condensation of 3,4-DHB-loaded AsbD with both primary amine isomers of spermidine (Figure 3 and B. F. Pfleger and D. H. Sherman, unpublished results), a result that is consistent with analysis of the Δ*asbA* and Δ*asbB* mutant strains of *B. anthracis* (*19*). This unexpected finding will require further exploration to establish the ultimate fate of this alternative accumulated intermediate.

In this study, we have confirmed the previously proposed (*19*) early steps in the petrobactin biosynthetic pathway by reconstitution of DHB-SP biosynthesis in vitro. We demonstrated the functional roles of AsbD, a new aryl carrier protein, AsbE, a condensing enzyme, and AsbC, the first 3,4-DHBA specific adenylation domain to be characterized in vitro. AsbC and its close homologues are unique compared to other adenylation domains at key binding domain residues (*41*), thereby defining a new A-domain family. Finally, we demonstrated that AsbC can be inhibited in vitro by an acylsulfamate analogue of 3,4-DHB-AMP with submicromolar affinity. Substrate specificity studies demonstrated the importance of the 3- and 4-hydroxyl groups on the phenyl ring. Future structure−activity relationship studies based on this strategy will focus on identification of inhibitors with improved potency for ultimate development of a *B. anthracis* specific antibiotic.

ACKNOWLEDGMENT

We thank Sabine Grüschow and Kathleen Noon for assisting with the LC−MS experimental design and data collection, as well as Brian K. Janes, Karla D. Passalacqua, and Nicholas Bergman for their expertise.

SUPPORTING INFORMATION AVAILABLE

Sequence clustering of aryl-adenylating enzymes (Figure 1). This material is available free of charge via the Internet at http://pubs.acs.org.

REFERENCES

1. Inglesby, T. V., O'Toole, T., Henderson, D. A., Bartlett, J. G., Ascher, M. S., Eitzen, E., Friedlander, A. M., Gerberding, J., Hauer, J., Hughes, J., McDade, J., Osterholm, M. T., Parker, G., Perl, T. M., Russell, P. K., and Tonat, K. (2002) Anthrax as a biological weapon, 2002: Updated recommendations for management, *J. Am. Med. Assoc. 287*, 2236−2252.
2. Dixon, T. C., Meselson, M., Guillemin, J., and Hanna, P. C. (1999) Anthrax, *N. Engl. J. Med. 341*, 815−826.
3. Leppla, S. H., Robbins, J. B., Schneerson, R., and Shiloach, J. (2002) Development of an improved vaccine for anthrax, *J. Clin. Invest. 110*, 141−144.
4. Brown, J. S., and Holden, D. W. (2002) Iron acquisition by Gram-positive bacterial pathogens, *Microbes Infect. 4*, 1149−1156.
5. Courcol, R. J., Trivier, D., Bissinger, M. C., Martin, G. R., and Brown, M. R. (1997) Siderophore production by *Staphylococcus aureus* and identification of iron-regulated proteins, *Infect. Immun. 65*, 1944−1948.
6. Finlay, B., and Falkow, S. (1997) Common themes in microbial pathogenicity revisited, *Microbiol. Mol. Biol. Rev. 61*, 136−169.
7. Ratledge, C., and Dover, L. G. (2000) Iron metabolism in pathogenic bacteria, *Annu. Rev. Microbiol. 54*, 881−941.
8. Ishimaru, C. A., and Loper, J. E. (1993) Biochemical and genetic analysis of siderophores produced by plant-associated strains of *Pseudomonas* spp. and *Erwinia* spp., in *Iron Chelation in Plants and Plant-Associated Microbial Systems* (Barton, L. L., and Hemming, B. C., Eds.) pp 27−73, Academic Press, New York.
9. Raymond, K. N., Dertz, E. A., and Kim, S. S. (2003) Enterobactin: An archetype for microbial iron transport, *Proc. Natl. Acad. Sci. U.S.A. 100*, 3584−3588.
10. Ratledge, C. (2004) Iron, mycobacteria and tuberculosis, *Tuberculosis (Edinburgh) 84*, 110−130.
11. Wandersman, C., and Delepelaire, P. (2004) Bacterial iron sources: From siderophores to hemophores, *Annu. Rev. Microbiol. 58*, 611−647.
12. Grass, G. (2006) Iron transport in *Escherichia coli*: All has not been said and done, *BioMetals 19*, 159−172.
13. Cendrowski, S., MacArthur, W., and Hanna, P. (2004) *Bacillus anthracis* requires siderophore biosynthesis for growth in macrophages and mouse virulence, *Mol. Microbiol. 51*, 407−417.
14. Rowland, B. M., Grossman, T. H., Osburne, M. S., and Taber, H. W. (1996) Sequence and genetic organization of a *Bacillus subtilis* operon encoding 2,3-dihydroxybenzoate biosynthetic enzymes, *Gene 178*, 119−123.
15. May, J. J., Wendrich, T. M., and Marahiel, M. A. (2001) The *dhb* operon of *Bacillus subtilis* encodes the biosynthetic template for the catecholic siderophore 2,3-dihydroxybenzoate-glycine-threonine trimeric ester bacillibactin, *J. Biol. Chem. 276*, 7209−7217.

16. Dertz, E. A., Xu, J., Stintzi, A., and Raymond, K. N. (2006) Bacillibactin-mediated iron transport in *Bacillus subtilis*, *J. Am. Chem. Soc. 128*, 22−23.
17. Koppisch, A. T., Browder, C. C., Moe, A. L., Shelley, J. T., Kinkel, B. A., Hersman, L. E., Iyer, S., and Ruggiero, C. E. (2005) Petrobactin is the primary siderophore synthesized by *Bacillus anthracis* str. Sterne under conditions of iron starvation, *BioMetals 18*, 577−585.
18. Wilson, M. K., Abergel, R. J., Raymond, K. N., Arceneaux, J. E., and Byers, B. R. (2006) Siderophores of *Bacillus anthracis*, *Bacillus cereus*, and *Bacillus thuringiensis*, *Biochem. Biophys. Res. Commun. 348*, 320−325.
19. Lee, J. Y., Janes, B. K., Passalacqua, K. D., Pfleger, B., Bergman, N. H., Liu, H., Hakansson, K., Somu, R. V., Aldrich, C. C., Cendrowski, S., Hanna, P. C., and Sherman, D. H. (2006) Biosynthetic analysis of the petrobactin siderophore pathway from *Bacillus anthracis*, *J. Bacteriol. 189*, 1698−1710.
20. Abergel, R. J., Wilson, M. K., Arceneaux, J. E., Hoette, T. M., Strong, R. K., Byers, B. R., and Raymond, K. N. (2006) Anthrax pathogen evades the mammalian immune system through stealth siderophore production, *Proc. Natl. Acad. Sci. U.S.A. 103*, 18499−18503.
21. Challis, G. L. (2005) A widely distributed bacterial pathway for siderophore biosynthesis independent of nonribosomal peptide synthetases, *ChemBioChem 6*, 601−611.
22. Finking, R., and Marahiel, M. A. (2004) Biosynthesis of nonribosomal peptides, *Annu. Rev. Microbiol. 58*, 453−488.
23. Crosa, J. H., and Walsh, C. T. (2002) Genetics and assembly line enzymology of siderophore biosynthesis in bacteria, *Microbiol. Mol. Biol. Rev. 66*, 223−249.
24. Burke, E., and Barik, S. (2003) Megaprimer PCR: Application in mutagenesis and gene fusion, *Methods Mol. Biol. 226*, 525−532.
25. Sanchez, C., Du, L., Edwards, D. J., Toney, M. D., and Shen, B. (2001) Cloning and characterization of a phosphopantetheinyl transferase from *Streptomyces verticillus* ATCC15003, the producer of the hybrid peptide-polyketide antitumor drug bleomycin, *Chem. Biol. 8*, 725−738.
26. Keating, T. A., Marshall, C. G., and Walsh, C. T. (2000) Vibriobactin biosynthesis in *Vibrio cholerae*: VibH is an amide synthase homologous to nonribosomal peptide synthetase condensation domains, *Biochemistry 39*, 15513−15521.
27. Copeland, R. A. (2005) *Evaluation of Enzyme Inhibitors in Drug Discovery: A Guide for Medicinal Chemists and Pharmacologists*, Wiley-Interscience, Hoboken, NJ.
28. Upson, R. H., Haugland, R. P., and Malekzadeh, M. N. (1996) A spectrophotometric method to measure enzymatic activity in reactions that generate inorganic pyrophosphate, *Anal. Biochem. 243*, 41−45.
29. Laursen, B., Denieul, M.-P., and Skrydstrup, T. (2002) Formal total synthesis of the PKC inhibitor, balanol: Preparation of the fully protected benzophenone fragment, *Tetrahedron 58*, 2231−2238.
30. Somu, R. V., Boshoff, H., Qiao, C., Bennett, E. M., Barry, C. E., III, and Aldrich, C. C. (2006) Rationally designed nucleoside antibiotics that inhibit siderophore biosynthesis of *Mycobacterium tuberculosis*, *J. Med. Chem. 49*, 31−34.
31. Lambalot, R. H., Gehring, A. M., Flugel, R. S., Zuber, P., LaCelle, M., Marahiel, M. A., Reid, R., Khosla, C., and Walsh, C. T. (1996) A new enzyme superfamily: The phosphopantetheinyl transferases, *Chem. Biol. 3*, 923−936.
32. McAllister, K. A., Peery, R. B., and Zhao, G. (2006) Acyl carrier protein synthases from Gram-negative, Gram-positive, and atypical bacterial species: Biochemical and structural properties and physiological implications, *J. Bacteriol. 188*, 4737−4748.
33. Copp, J. N., and Neilan, B. A. (2006) The Phosphopantetheinyl transferase superfamily: Phylogenetic analysis and functional implications in cyanobacteria, *Appl. Environ. Microbiol. 72*, 2298−2305.
34. Quadri, L. E., Weinreb, P. H., Lei, M., Nakano, M. M., Zuber, P., and Walsh, C. T. (1998) Characterization of Sfp, a *Bacillus subtilis* phosphopantetheinyl transferase for peptidyl carrier protein domains in peptide synthetases, *Biochemistry 37*, 1585−1595.
35. Ehmann, D. E., Shaw-Reid, C. A., Losey, H. C., and Walsh, C. T. (2000) The EntF and EntE adenylation domains of *Escherichia coli* enterobactin synthetase: Sequestration and selectivity in acyl-AMP transfers to thiolation domain cosubstrates, *Proc. Natl. Acad. Sci. U.S.A. 97*, 2509−2514.
36. Gehring, A. M., Mori, I., Perry, R. D., and Walsh, C. T. (1998) The nonribosomal peptide synthetase HMWP2 forms a thiazoline ring during biogenesis of yersiniabactin, an iron-chelating virulence factor of *Yersinia pestis*, *Biochemistry 37*, 11637−11650.
37. Rusnak, F., Faraci, W. S., and Walsh, C. T. (1989) Subcloning, expression, and purification of the enterobactin biosynthetic enzyme 2,3-dihydroxybenzoate-AMP ligase: Demonstration of enzyme-bound (2,3-dihydroxybenzoyl)adenylate product, *Biochemistry 28*, 6827−6835.
38. Vannada, J., Bennett, E. M., Wilson, D. J., Boshoff, H. I., Barry, C. E., III, and Aldrich, C. C. (2006) Design, synthesis, and biological evaluation of β-ketosulfonamide adenylation inhibitors as potential antitubercular agents, *Org. Lett. 8*, 4707−4710.
39. Ferreras, J. A., Ryu, J. S., Di Lello, F., Tan, D. S., and Quadri, L. E. (2005) Small-molecule inhibition of siderophore biosynthesis in *Mycobacterium tuberculosis* and *Yersinia pestis*, *Nat. Chem. Biol. 1*, 29−32.
40. Somu, R. V., Wilson, D. J., Bennett, E. M., Boshoff, H. I., Celia, L., Beck, B. J., Barry, C. E., III, and Aldrich, C. C. (2006) Antitubercular nucleosides that inhibit siderophore biosynthesis: SAR of the glycosyl domain, *J. Med. Chem. 49*, 7623−7635.
41. May, J. J., Kessler, N., Marahiel, M. A., and Stubbs, M. T. (2002) Crystal structure of DhbE, an archetype for aryl acid activating domains of modular nonribosomal peptide synthetases, *Proc. Natl. Acad. Sci. U.S.A. 99*, 12120−12125.
42. Quadri, L. E., Sello, J., Keating, T. A., Weinreb, P. H., and Walsh, C. T. (1998) Identification of a *Mycobacterium tuberculosis* gene cluster encoding the biosynthetic enzymes for assembly of the virulence-conferring siderophore mycobactin, *Chem. Biol. 5*, 631−645.
43. Barbeau, K., Zhang, G., Live, D. H., and Butler, A. (2002) Petrobactin, a photoreactive siderophore produced by the oil-degrading marine bacterium *Marinobacter hydrocarbonoclasticus*, *J. Am. Chem. Soc. 124*, 378−379.
44. Larimer, F. W., Chain, P., Hauser, L., Lamerdin, J., Malfatti, S., Do, L., Land, M. L., Pelletier, D. A., Beatty, J. T., Lang, A. S., Tabita, F. R., Gibson, J. L., Hanson, T. E., Bobst, C., Torres, J. L., Peres, C., Harrison, F. H., Gibson, J., and Harwood, C. S. (2004) Complete genome sequence of the metabolically versatile photosynthetic bacterium *Rhodopseudomonas palustris*, *Nat. Biotechnol. 22*, 55−61.
45. Banwell, M. G., Crasto, C. F., Easton, C. J., Forrest, A. K., Karoli, T., March, D. R., Mensah, L., Nairn, M. R., O'Hanlon, P. J., Oldham, M. D., and Yue, W. (2000) Analogues of SB-203207 as inhibitors of tRNA synthetases, *Bioorg. Med. Chem. Lett. 10*, 2263−2266.

BI6023995